Journal of Physics D:
Applied Physics

PURPOSE-LED PUBLISHING™

PAPER • **OPEN ACCESS**

Investigation of N_2/O_2 plasma interaction with Pt-catalyst: effect of metastable adsorbates on product hysteresis

To cite this article: Michael Hinshelwood and Gottlieb S Oehrlein 2025 *J. Phys. D: Appl. Phys.* **58** 165203

View the article online for updates and enhancements.

You may also like

- Quadratic magneto-optical Kerr effect spectroscopy: polarization variation method for investigation of magnetic and magneto-optical anisotropies
V Wohlrath, Z Sadeghi, J Kimák et al.
- Miniaturized near-field polarization photodetector
Yingshuang Zheng, Fei Zhu, Chunqi Jin et al.
- Numerical modelling of wire arc additive manufacturing: methods, status, trends, and opportunities
Yun H Kim, Dayalan R Gunasegaram, Paul W Cleary et al.

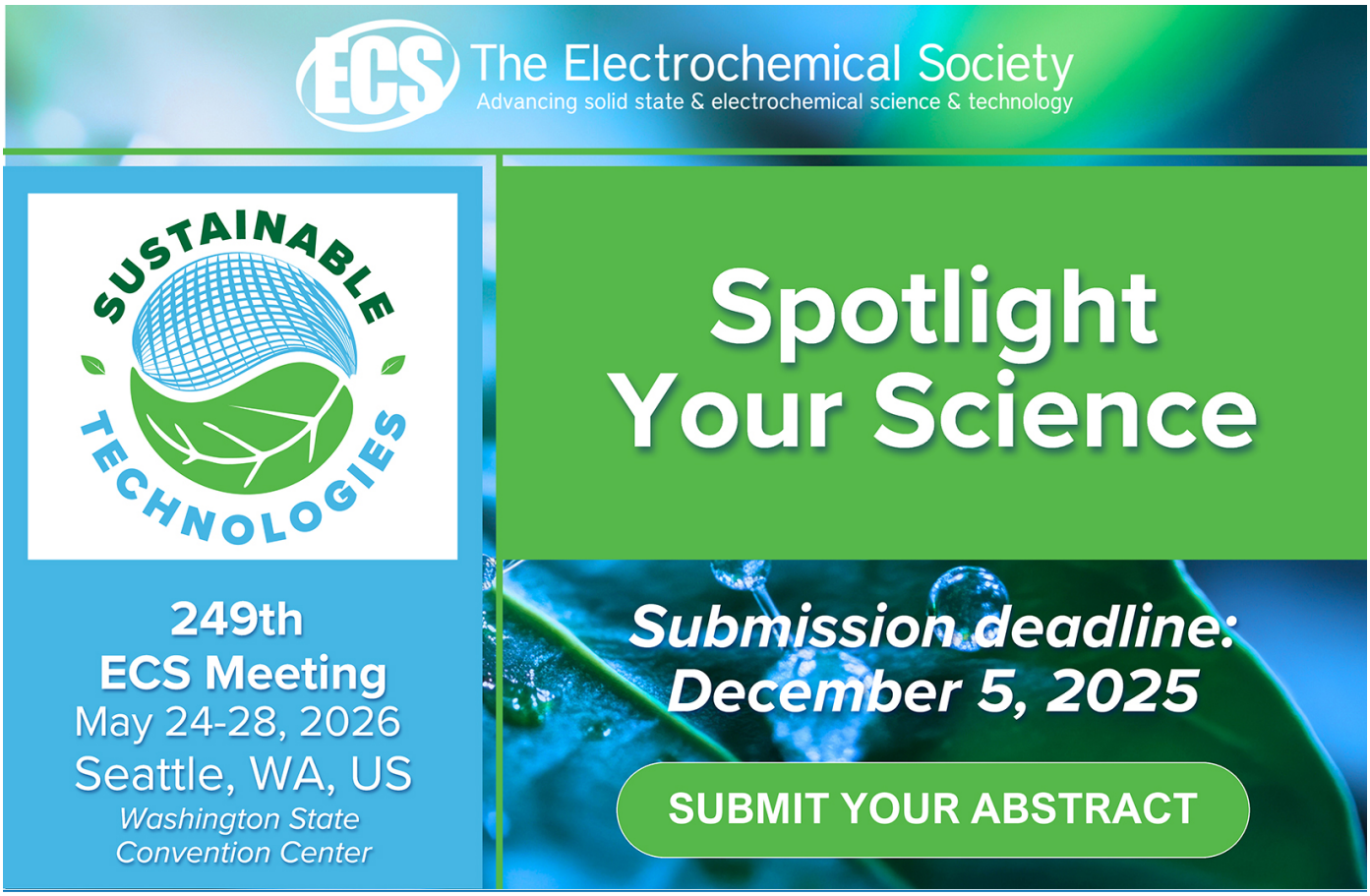

This content was downloaded from IP address 172.56.3.220 on 30/11/2025 at 21:07

OPEN ACCESS
IOP Publishing
Journal of Physics D: Applied Physics
J. Phys. D: Appl. Phys. **58** (2025) 165203 (17pp)
https://doi.org/10.1088/1361-6463/adb9f8

Investigation of N_2/O_2 plasma interaction with Pt-catalyst: effect of metastable adsorbates on product hysteresis

Michael Hinshelwood and Gottlieb S Oehrlein*

Department of Materials Science and Engineering and the Institute for Research in Electronics and Applied Physics, University of Maryland, College Park, MD 20742, United States of America

E-mail: oehrlein@umd.edu

Received 25 November 2024, revised 6 February 2025
Accepted for publication 25 February 2025
Published 12 March 2025

Abstract

The coupling of catalysts and atmospheric-pressure plasma has the potential to improve the efficiency of certain catalytic reactions. Understanding the changes that the catalyst surface undergoes during exposure to plasma is key to improving plasma–catalytic performance. In this work, long term exposure of Pt–Al_2O_3 powder catalyst to an Ar/N_2/O_2 non-equilibrium atmospheric-pressure plasma-jet was investigated. Products produced by the interaction were analyzed downstream with Fourier-transform infrared spectroscopy while surface species were analyzed *operandi* with diffuse reflectance infrared Fourier transform spectroscopy. During exposure, the catalyst temperature was ramped cyclically between 100 °C and 350 °C to understand how substrate temperature affects the plasma–catalyst interaction. Long-lasting changes were revealed to take place on the catalyst surface during plasma exposure. At low temperatures, Pt–O and Pt–NO accumulate on the surface which react at elevated temperatures to form NO_2. NO_2 initially appears to spill on to the Al_2O_3 support as nitrites and nitrates instead of desorbing. Stable surface conditions are only achieved after prolonged plasma exposure, when nitrate sites on the Al_2O_3 support are filled. By changing the catalyst temperature at various rates, the impact of total plasma species flux to the surface was analyzed. It was found that decreasing the heating rate increased the hysteresis in the pattern of NO_2 formation during thermal cycling. The variation with temperature demonstrates that plasma exposure results in a buildup of surface NO_x and oxygen species which react or desorb at high temperatures. The observed changes are discussed from the generic viewpoint that a non-equilibrium plasma interacting with a catalyst at low temperature introduces metastable steady-state surface conditions. Upon heating above a threshold temperature, the introduced surface modifications can change either due to thermal effects, or, for a plasma environment, by additional interaction with the incident plasma species flux. The surface/material changes take place in a highly predictable fashion and after sufficient time above the threshold temperature reach a steady-state condition that is different from the transient behavior that is observed during initial heating. During cooling the plasma-surface interaction exhibits a different behavior than during heating, and this results in hysteresis of diverse observables. The metastability/hysteresis description appears quite generic and analogous to hysteresis behavior

* Author to whom any correspondence should be addressed.

© 2025 The Author(s). Published by IOP Publishing Ltd

Original content from this work may be used under the terms of the Creative Commons Attribution 4.0 licence.
Any further distribution of this work must maintain attribution to the author(s) and the title of the work, journal citation and DOI.

seen for different systems. It is expected to be useful for understanding the consequences of plasma–catalyst surface interactions for various systems.

Keywords: investigation, N_2/O_2, plasmas, interactions, Pt, catalysts

1. Introduction

Hysteresis is a generic phenomenon prevalent across a wide range of systems, from magnetic hysteresis in ferromagnetic and piezoelectric materials to biological cell responses [1–3]. A non-equilibrium phenomenon, hysteresis indicates a dependence of the state of a system on its history. This dependence can create a loop-like behavior in the system's response to continuous changes in a given parameter, as seen in figure 1. These loops may be symmetric, such as in the response of ferromagnetic materials to a magnetizing force, or asymmetric, which is typical of temperature-based hysteresis [1]. Hysteresis is commonly seen in catalytic systems and can lead to complex reaction pathways and non-linear behavior in catalytic processes, impacting the overall efficiency and selectivity of the reaction. Absorption–desorption mechanisms, critical in catalysis, may exhibit hysteresis. For example, gas adsorption on a porous surface when subject to varying pressures may show a different pattern from desorption, the degree of which is influenced by temperature [4, 5]. Temperature hysteresis during catalytic conversion of gases is often seen, particularly for exothermic reactions [6]. Oxidation reactions, such as the oxidation of CO or NO over noble catalysts, have been known to exhibit both regular and inverse hysteresis [7–9]. In regular hysteresis, the catalytic activity is greater during the cooling phase of the temperature loop, while the opposite is true for inverse-hysteresis. In these and other oxidation systems, such as the oxidation of CH_4 over Pt–Al_2O_3, changes in the oxidation state of the catalyst is often thought to be critical to the hysteresis effect [10].

Hysteresis is closely tied with the concept of metastability. Metastability refers to the state of a system existing in a configuration that is not the most thermodynamically stable yet persists over time due to free energy barriers hindering it from transitioning to a more stable state [11]. Should the system overcome the free-energy barrier, it will spontaneously move to a more stable configuration. Metastability can give rise to hysteresis as asymmetrical behavior since in response to increasing and decreasing temperature it creates a hysteresis loop. Metastable materials may possess unique properties that deviate from those of their stable counterparts, making them desirable for various applications. Low-temperature plasma processing has long been known as a tool for creating metastable material surfaces and films. The non-equilibrium nature of the plasma allows for a particle flux arriving at a surface to produce a state that would normally require high temperatures to create. For instance, corrosion resistance of steel can be improved by the formation of metastable nitrided austenite layer that must be formed below 450 °C [12]. Such a layer can be produced by low temperature nitrogen plasma exposure. Other examples with low temperature plasma include the production of diamond films [13], or the production of amorphous silicon and its passivated counterpart amorphous hydrogenated silicon (a-Si:H). a-Si:H is widely used in electronics and photovoltaics [14], and may be promising for as a photonic material due to the ability to induce metastable refractive index changes in the material [15].

The combination of low temperature plasma and catalysis, plasma catalysis, involves the coupling of heterogeneous catalytic reaction systems with plasma. It is likely to heavily display examples of metastable surfaces and hysteresis. The plasma generates a range of excited species—from atomic radicals to photons—which can interact with the catalyst to reduce reaction activation energies or boost product yields [16, 17]. Non-equilibrium, or cold, plasma is particularly suited to plasma catalysis due to the much lower gas temperature compared to thermal plasma [18, 19]. This allows for greater temperature control in the catalytic reaction and greater catalyst stability within the reaction environment. Plasma–catalyst interactions can be complex due to the variety of species reaching the catalyst. Other surface changes, such as particle dispersion, may alter catalyst morphology [20, 21]. Some surface changes may persist post-plasma exposure, permanently changing catalyst reactivity [22]. Plasma–catalyst synergy is typically thought to occur when plasma combined with a catalyst outperforms each method used separately. Such synergy has been demonstrated for a variety of plasma–catalytic systems [23–27].

One system of great importance is that of nitrogen fixation, the conversion of stable nitrogen gas into reactive nitrogen-based compounds. This process is critical for fertilizer production and world-wide agriculture. Currently, nitrogen fixation is primarily achieved via the Haber–Bosch method for ammonia synthesis via N_2 and H_2 [28]. The desire for more eco-friendly processes has driven research towards electrically driven methods of nitrogen fixation. Many different catalytic techniques are being evaluated, from enzymatic to electrolytic catalysis [28, 29].

For nitrogen fixation, plasma catalysis has been applied to two reactions: combining N_2 with H_2 to form ammonia (NH_3), and N_2 with O_2 to produce nitrogen oxides (NO_x), both crucial for fertilizer production through nitrates. The generation of NO_x solely by plasma is a long-established concept, from the development of the Birkeland–Eyde process [30]. Plasma

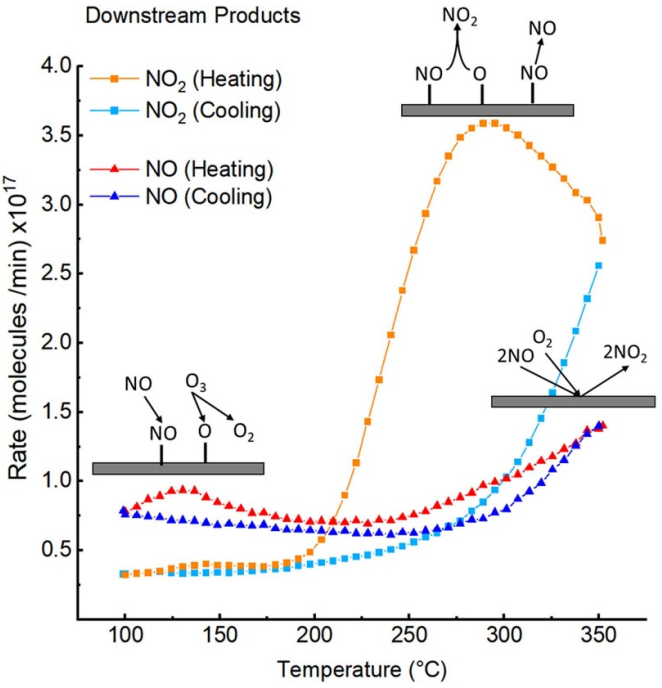

Figure 1. Diagram illustrating a hysteresis loop in the production of NO_2 and NO during N_2/O_2 plasma exposure to Pt–Al_2O_3 catalyst. The production during heating is higher than during cooling for equivalent temperatures.

allows for the formation of NO_x through the Zeldovich mechanism under more favorable conditions by creating atomic N and O through electron impact dissociation at atmospheric pressure [31].

Plasma generation of NO_x was not able to compete with the Haber–Bosch process from an efficiency standpoint [30]. However, introducing a catalyst into the reaction system can lead to efficiency improvements. Studies have demonstrated efficiency enhancements in NO_x production for plasma catalyst systems with either very close coupling, or sub-atmospheric pressures [32–34]. Understanding the adsorbate surface coverages which form due to plasma exposure, as well as the way these adsorbates react, is difficult. Significant technical difficulties exist in integrating diagnostics in plasma–catalyst systems at atmospheric or near-atmospheric pressure and traditional surface science techniques are often incompatible with such conditions [23, 35]. Additionally, the reactivity of surface adsorbates changes with catalyst temperature, as does the adsorption characteristics of the catalyst itself [36, 37]. This makes variation of the catalyst temperature an important variable for tailoring reaction systems.

Overall, while plasma catalysis offers a promising avenue for environmentally friendly nitrogen fixation, a deeper understanding of the surface reactions is essential for further advancements. Understanding how catalytic surfaces change during long term exposure to nitrogen and oxygen plasmas is especially important if they are to be used in industrial settings. This is true for plasma catalysis generally, and the development of broader frameworks for understanding of such reaction systems will help increase the overall understanding of plasma catalyst interactions.

In a prior study [38], characterization techniques were utilized which allow for *in-situ* characterization of plasma–catalyst interactions [39]. The coupling of an $Ar/N_2/O_2$ atmospheric pressure plasma jet with a Pt–Al_2O_3 catalyst was investigated with a focus on the changes to downstream products due to the catalyst. NO and O_3 were assessed to be the primary reactive species fluxes to the catalyst, as short-lived radicals such as O or N are unlikely to reach the surface. While no enhancement of nitrogen oxidation due to plasma catalytic coupling was seen, the catalyst was found to greatly increase the O/N ratio in the products at high temperature due to oxidation of plasma produced NO on the Pt surface. Thermal cycling of the catalyst under plasma exposure revealed a hysteresis pattern with elevated product formation at high temperatures. This was thought to be due to low temperature adsorption of reactive species and their subsequent reaction upon substrate temperature increase.

A schematic overview of this hysteresis is shown in figure 1 showing the assumed potential pathways of NO through the system based on catalyst temperature. At low temperatures, NO produced in the plasma arrives at the catalyst surface. Some passes through the catalyst bed and is measured in the downstream products, while some is adsorbed on the Pt surface as Pt–NO or potentially destroyed through surface recombination. At high temperatures, the NO which at low temperature would adsorb and remain will instead quickly be oxidized or desorb depending on the availability of oxygen. This leads to a larger amount of NO_2 and NO in the downstream product measurements.

The NO which is adsorbed at low temperatures will leave the surface as the catalyst temperature is increased leaving the catalyst with greatly reduced adsorbate surface coverage. Whether it leaves as NO or reacts with oxygen to form NO_2 depends on the oxygen availability of the system which results from O_2 or O_3 flux to the surface. The degree of NO oxidation or loss depends on the plasma conditions which govern the flux composition to the surface.

Pt–O surface coverage was found to be crucial for achieving a high NO_2 ratio in the downstream products during hysteresis. Thermal cycling of the catalyst resulted in an additional oxidation mechanism at high temperature, from the reaction of previously formed Pt–NO and Pt–O, in addition to steady state reaction of incoming species at high temperature.

In this work, we build on the prior analysis, focusing on the observed hysteresis effect seen with this plasma catalyst coupling. The pattern of NO and NO_2 production during hysteresis was analyzed versus both time and temperature for different rates of heating and cooling. Correlation of downstream products and surface species during thermal cycling revealed that long-lasting changes take place during the first cycles, due to the stabilization of the surface and the filling of sites on the Al_2O_3 support. The degree of hysteresis is influenced by the total flux to the surface at low temperature and the build-up of Pt–O. The observed reaction patterns can be described as the formation of metastable surface coverages which lead to hysteresis of NO_x production during catalyst heating and

cooling. Specifically, the non-equilibrium plasma can impart a metastable adsorbate composition on the catalyst surface at low temperature. The highly predictable patterns observed for reaction products during plasma exposure appear to be characteristic for the field of plasma catalysis and plasma-surface interactions in general.

2. Experimental design

2.1. Apparatus for plasma generation

Figure 2 illustrates the experimental apparatus, an atmospheric pressure plasma jet (APPJ) of the annular-ring, dielectric-barrier discharge geometry. The APPJ consists of a 1 mm diameter tungsten pin inside a quartz tube with a 3 mm inner diameter. A copper ring is placed around the tube's end, serving as the ground electrode. Specifications of the jet are detailed in previous literature [40–42]. The jet operated at a frequency of 14.3 MHz with a 20% duty cycle, a configuration utilized for its power efficiency in similar gas conditions [23].

Two gas mixtures were used herein. The first, similar to air, contained 2.5 sccm N_2, 0.5 sccm O_2, and 200 sccm Ar. The second, richer in O_2, had 0.5 sccm N_2, 2.0 sccm O_2, and 200 sccm Ar. These configurations are referred to as N_2-rich and O_2-rich, respectively. The plasma operated mainly at 2 W or 3.5 W power. Plasma power was calculated by isolating it from the circuit's total power, as described by Li *et al* [23].

2.2. Reaction chamber and catalytic material

Our experiments utilized a high-temperature reaction chamber from Harrick Scientific, modified for our purposes and previously described in detail [23, 39]. The chamber contains a stainless-steel holder for the catalyst powder, equipped with a heating mechanism and a thermocouple for catalyst temperature monitoring. It features water cooling and a lid with three apertures: two for diffuse reflectance infrared Fourier transform spectroscopy (DRIFTS) and another for the APPJ. The plasma-generated species interact with the catalyst, situated 5 mm from the nozzle, and the composition of these species varies with the operational parameters. The time for a gas molecule to travel from the nozzle to the catalyst is about 40 ms at our operational flow rates (200 sccm).

We used a 5 wt% Pt on γ-Al_2O_3 catalyst from Sigma Aldrich, product number 205974. This catalyst has a reported surface area of approximately 100 $m^2\ g^{-1}$ and a Pt particle diameter of about 5 nm [43, 44]. The Al_2O_3 particles, ranging between 37 and 74 μm in diameter, were contained using a stainless-steel mesh.

2.3. Gas analysis and surface examination

Two main characterization approaches were used: surface analysis and downstream gas species characterization. Downstream gas species characterization used a Shimazdu IR-Tracer 100 FTIR spectrometer with an MCT detector, coupled with a 16 m path-length gas cell from Pike Technologies. The gas from the chamber mixed with 1 slm Ar to shorten residence time in the gas cell, with a total transfer time of around 2 s from reactor to measurement cell. The FTIR spectra were recorded at 0.5 cm^{-1} resolution, averaging 10 scans. Gas species densities were quantified using IR cross-section data from the HITRAN database [45]. For *in-situ* surface analysis, DRIFTS was utilized. A compartment from Harrick Scientific was used to hold the previously described reaction chamber, all incorporated into the same FTIR spectrometer. The chamber's lid has KBr windows to allow IR light transmission. DRIFTS spectra were recorded at 4 cm^{-1} resolution, averaging 20 scans for optimal signal-to-noise balance. The DRIFTS analysis provides qualitative data, as precise calibration for adsorbate surface coverage was not available. Both DRIFTS and gas analysis were conducted in real-time. Prior to any experiment, the gas lines were evacuated to 10^{-5} torr and purged the chamber with Ar for 30 min.

For thermal cycling experiments, the powder bed was first exposed to plasma at 100 °C for 5 min, then heated under plasma from 100 °C to 350 °C at set ramp rates, with a minute's dwell at each temperature extreme. 5 °C min^{-1}, 10 °C min^{-1}, and 15 °C min^{-1} were used as the ramp rates, to understand how a larger total flux to the surface at each temperature affected the reaction. When employing multiple thermal cycles, the cycles were conducted continuously, one after the other. We ensured the catalyst temperature did not exceed 350 °C to prevent the formation of gaseous platinum oxide, which could contaminate the setup [46–49].

3. Experimental results

3.1. Gas-phase characterization of downstream products

Gas phase characterization was conducted to analyze and measure the products generated by the plasma–catalytic reaction. Figure 3 provides an illustration of FTIR spectra representing the gases produced downstream when Pt–Al_2O_3 was exposed to plasma during thermal cycling. These spectra were recorded under oxygen rich conditions with a plasma power of 3.5 W. Under all conditions presented in this work, only three distinct reactive oxygen–nitrogen species (RONS) were observed in the product gas: NO_2, NO, and N_2O. Other species like O_3, N_2O_5, and HNO_3 appeared at lower power levels in oxygen-rich conditions, but those conditions were not used here. The spectral peaks were converted into concentrations using Beer's law, as shown in equation (3.1):

$$A = xlC \tag{3.1}$$

where C is the concentration, x the IR cross section, A absorbance, and l is the total IR path length.

IR cross sections for the respective species were obtained through the HITRAN database [45].

Scan to scan variation for constant gas densities is minimal. Nevertheless, there could be some inaccuracies in measuring the quantity as the gas densities were not adjusted using a

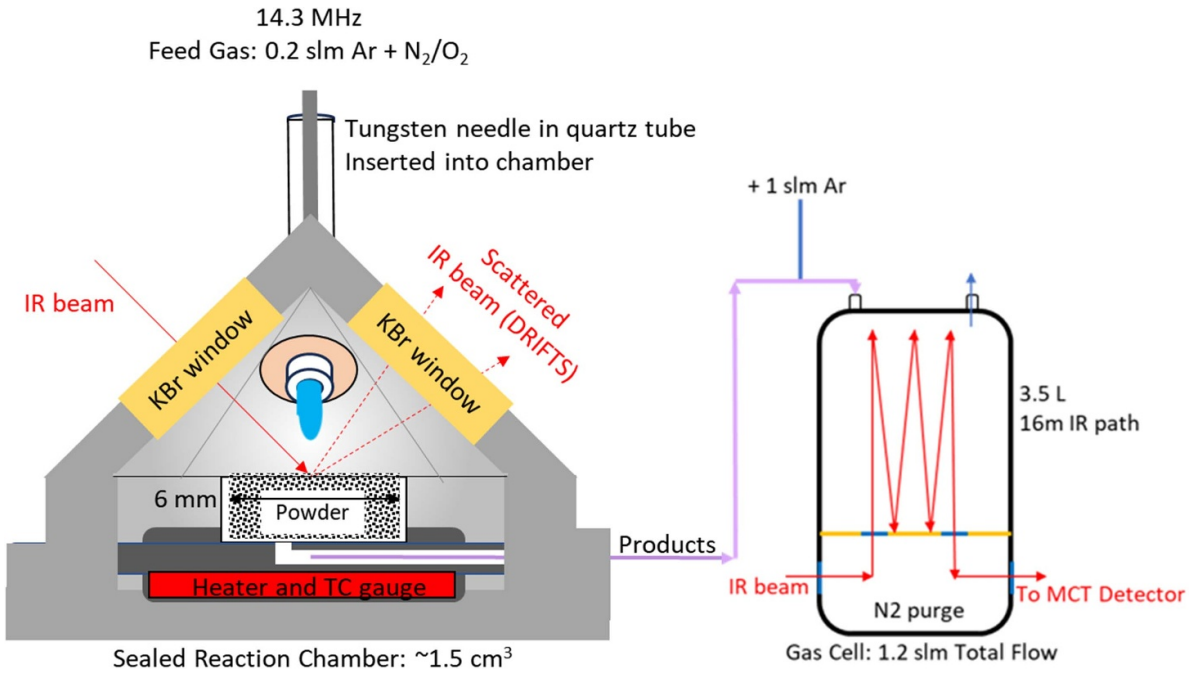

Figure 2. Plasma catalyst reactor diagram. Nozzle orifice to powder distance is 5 mm. Adapted from [38]. © IOP Publishing Ltd. All rights reserved.

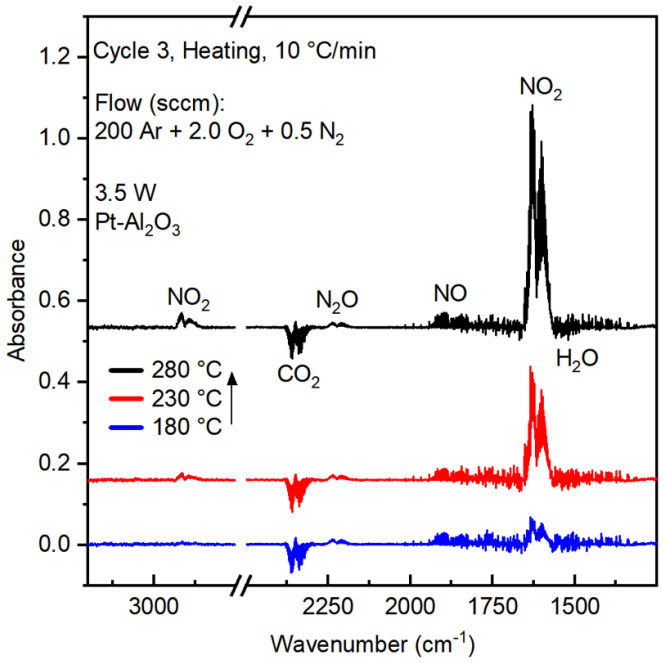

Figure 3. FTIR example spectra of downstream gas products during the heating section of a thermal cycle with a 10 °C min^{-1} ramp rate. Spectra from the third thermal cycle under O_2 rich plasma exposure to Pt–Al_2O_3 are shown.

standard calibration gas. Therefore, this paper mainly examines the relative changes in the densities of products.

Infrared signatures related to CO_2 and H_2O are noticeable under all tested conditions. These are likely due to minor atmospheric impurities and are not examined further in this study. RONS are not observed in the absence of plasma, across all tested catalyst temperatures and gas flow scenarios. This aligns with expectations, given that the catalyst temperatures used in this study are too low to induce thermal formation of nitrogen oxides (NO) [33].

3.2. *Effect of thermal cycling on downstream product densities*

The primary testing method employed in this work was thermal cycling of the catalyst powder under plasma exposure. This was done to ascertain the role of catalyst temperature on the plasma catalyst interaction, especially the effect on surface adsorbates. This experimental procedure involved repetitive thermal cycling of the catalyst material from 100 °C to 350 °C at various ramp rates with continuous cycling. The choice of 100 °C as the lower limit was based on the limitation of the reaction chamber's cooling system, which cannot maintain a cooling rate of 10 °C min^{-1} below this temperature. Furthermore, the temperature range was selected considering that 100 °C is below the threshold for NO oxidation on Pt surfaces, while 350 °C exceeds it [50]. This technique of thermal cycling has been applied to the study of catalysis for NO_x abatement in both thermal and plasma catalytic systems [51–53].

Figure 4 shows downstream NO_2 and NO products during thermal cycling under constant exposure to N_2 rich plasma for both Pt–Al_2O_3 and Al_2O_3. Downstream products with Pt–Al_2O_3 show temperature dependent formation, with NO_2 and NO densities rising rapidly at 280 °C to form a hysteresis loop. Additionally, the hysteresis loop changes across the first three cycles. Initially almost no temperature dependence is seen, and downstream product densities of both NO and NO_2 are low

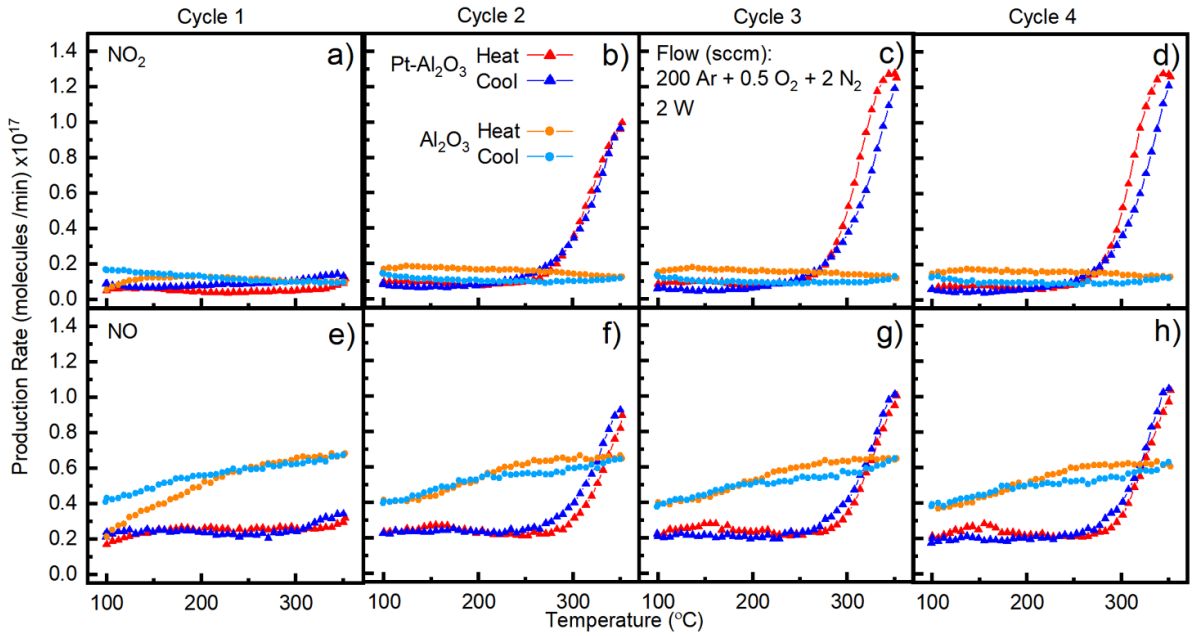

Figure 4. Densities of downstream products during thermal cycling of Pt–Al_2O_3 or Al_2O_3 under constant plasma exposure. 10 °C min^{-1} was used as the heating and cooling rate. Cycles were consecutive with no gap in between. Product formation rate shows stronger temperature dependence with Pt–Al_2O_3 than Al_2O_3. (a)–(d) NO_2 cycles 1–4. (e)–(h) NO cycles 1–4. Cycle 3 of these results was presented in [38].

throughout. After three cycles, the pattern becomes consistent, with the third and fourth cycle being identical. This is not the case for Al_2O_3 which has a near identical pattern for all four cycles. Downstream products with Al_2O_3 do not show a strong temperature dependence. This strong hysteresis effect is due to the presence of Pt which is known to catalyze the release of adsorbed NO_x on the catalyst surface [54, 55]. These differences are further described in [38].

Figure 5 shows a similar experiment, but for O_2 rich plasma over Pt–Al_2O_3 at either 2 or 3.5 W dissipated power. In both cases temperature dependent product formation is much stronger than for N_2 rich plasma. Increasing power clearly increases the size of the hysteresis loops between 2 and 3.5 W. 3.5 W O_2 rich plasma also reaches repeatable hysteresis conditions one cycle before 2 W O_2 or N_2 rich plasma, with cycles 2–4 being identical for both NO_2 and NO. A dip in NO production occurs at around 230 °C during cycle 1 for O_2 rich 3.5 W plasma. This may indicate the catalyst becoming active for NO oxidation; however, it does not occur in the next three cycles which are extremely similar.

To investigate the dependence of adsorbate surface coverage on product formation temperature, thermal cycling was performed at various heating rates for 3.5 W O_2 rich plasma, shown in figures 6 and 7. Figures 6 and 7 show the same experiment, heating from 100 °C to 350 °C and back, plotted vs temperature (figure 6) or time (figure 7). Theoretically, with a lower ramp rate, more reactive species would arrive at the surface during the span of the thermal cycle, resulting in a higher adsorbate surface coverage.

For O_2 rich plasma, densities of both NO and NO_2 have a consistent pattern during catalyst cooling across both temperature and time. NO_2 heating curves change significantly with the heating rate, with the temperature of product-formation increase lowering as the heating rate drops. From 15 °C min^{-1} to 5 °C min^{-1} the temperature of NO_2 increase drops around 100 °C. However, the start time of this increase is consistent for each heating rate. NO heating curves remain broadly similar across temperature for different heating rates.

The rolling-sum totals of produced NO and NO_2 are also shown in figures 6 and 7. Total NO_x produced during heating nearly doubles when the heating rate is halved. This is understandable, as when the heating rate is halved, the ratio of time spent at low and high temperature is the same, though it suggests that most of the adsorbed reactants are depleted in both cases. Additionally, the initial generation of NO is determined by the plasma, and the catalyst is not expected to have a major effect on NO generation or destruction in the experimental configuration used here.

Surface analysis during thermal cycling was employed to understand what surface processes take place during the prominent hysteresis visible in the downstream product measurements. Figures 8(a) and (b) show surface species evolution during the first thermal cycling of Pt–Al_2O_3 or Al_2O_3 under 2 W N_2-rich plasma. The negative peak at 1670 cm^{-1} is attributed to water [39]. The peak at 1770 cm^{-1} is thought to be due to NO adsorbed on platinum [54, 56]. The peaks in the 1000–1600 region are due to nitrites and nitrates adsorbed on Al_2O_3. 1550 cm^{-1} and 1255 cm^{-1} are believed to be

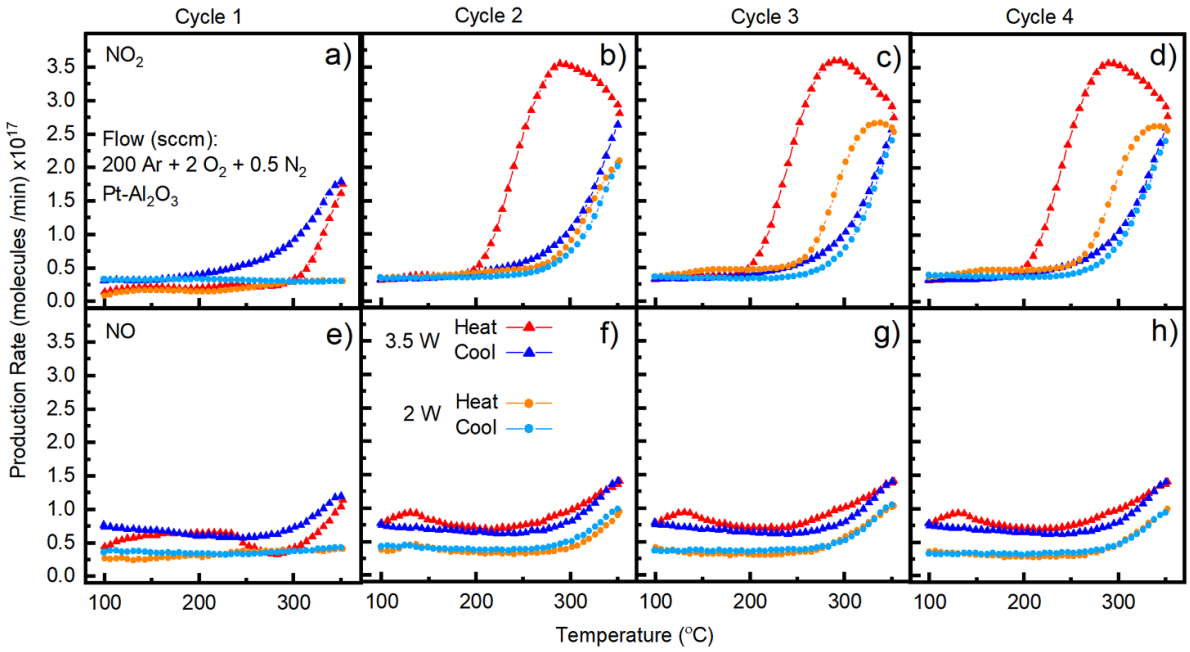

Figure 5. Production rate of downstream products during thermal cycling of Pt–Al_2O_3 under constant plasma exposure at either 2 or 3.5 W. O_2 rich plasma gas conditions. 10 °C min^{-1} was used as the heating and cooling rate. Cycles were consecutive with no gap in between. Hysteresis effects reach consistency faster with higher power. (a)–(d) NO_2 cycles 1–4. (e)–(h) NO cycles 1–4. Cycle 3 of these results was presented in [38].

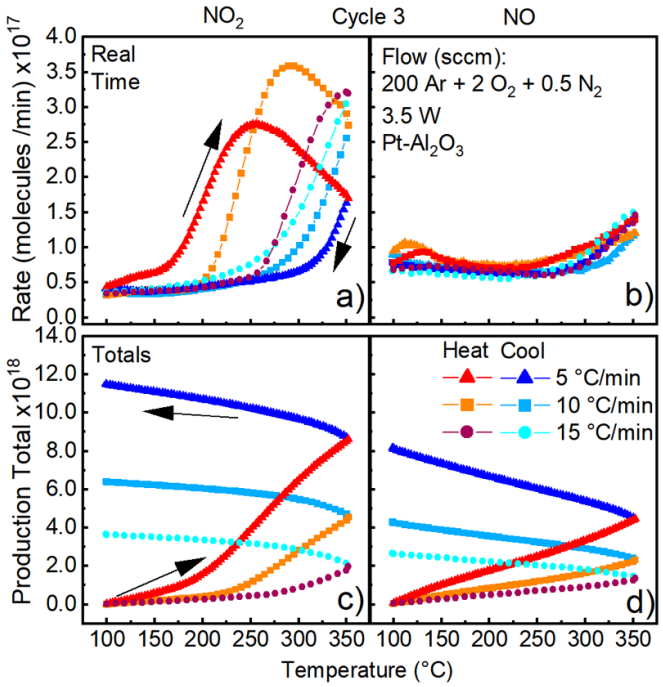

Figure 6. Densities of downstream products during thermal cycling of Pt–Al_2O_3 under 3.5 W O_2-rich plasma at various temperature ramp rates. Densities are plotted versus catalyst temperature. Cycles were consecutive with no gap in between; the third cycle is shown. (a) NO_2 production rate. (b) NO production rate. (c) Rolling sum NO_2. (d) Rolling sum NO.

monodentate nitrate [54, 56–62], 1313 cm^{-1} bidentate nitrate [59, 60], and 1235 cm^{-1} bidentate nitrite [57, 60, 62–66]. Peaks at 1440 cm^{-1} and 1350 cm^{-1} are likely due to forms of solvated nitrate from interaction with water [63, 67–70]. For the purposes of this work, only the surface peaks during the first thermal cycle are analyzed. Discussion of subsequent cycles when downstream hysteresis becomes consistent can be found in [38].

The same nitrate peaks occur on both materials and Pt–NO only occurs on Pt–Al_2O_3. Solvated nitrate peaks appear to decrease with substrate temperature, likely from water desorbing from the Al_2O_3. The nitrate buildup is different for the catalyst and support during the first heating curve. For Al_2O_3 the nitrates build up steadily, while for Pt–Al_2O_3 a sharp increase occurs around 225 °C. This is easily visible for the 1550 cm^{-1} peak (figure 8(b)).

Figure 8(c) shows the first cycle for 2 W O_2 rich plasma over Pt–Al_2O_3. For O_2 rich plasma, nitrates build up rapidly on the support surface. There may be a Pt–NO peak at 1770 cm^{-1}, however it is very slight. Solvated nitrate is less prominent, suggesting that O_2 rich plasma may enhance water removal.

4. Discussion

4.1. Transient and long-lasting surface changes during plasma exposure

The species flux to the catalyst surface was assessed to be primarily NO and O_3, based on the parameters of our reaction apparatus and data in the literature from similar systems [42, 71–74]. The exact fluxes to the surface change with plasma feed gas and plasma power. For systems with closer coupled plasma and catalyst, the reaction system would likely

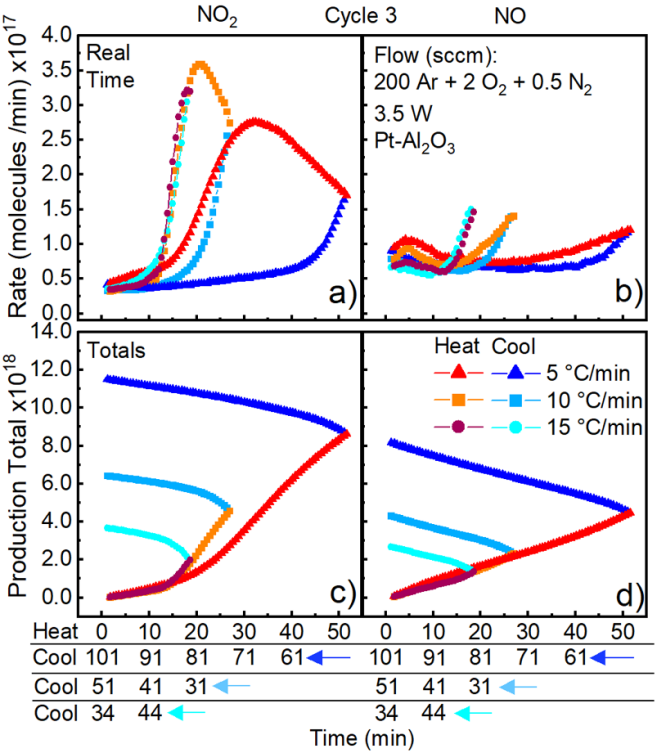

Figure 7. Densities of downstream products during thermal cycling of Pt–Al_2O_3 under 3.5 W O_2-rich plasma at various temperature ramp rates. Densities are plotted versus exposure time. The top row of the x-axis is the time during heating to 350 °C, next row is cooling at 5 °C min^{-1}, then cooling at 10 °C min^{-1}, then cooling at 15 °C min^{-1}. Cycles were consecutive with no gap in between; the third cycle is shown. (a) NO_2 production rate. (b) NO production rate. (c) Rolling sum NO_2. (d) Rolling sum NO.

be expanded to include radical and excited molecular species. A more detailed description can be found in [38].

A change in hysteresis pattern across the first few thermal cycle loops is visible in figure 4. In the first cycle, the amount of NO_x formed downstream at high catalyst temperatures is low, and almost none for both Pt–Al_2O_3 and Al_2O_3. In subsequent cycles, NO_x density at high temperatures for Pt–Al_2O_3 increases and the hysteresis loops become quite stable and reproducible. There is no evidence of plasma produced species changing over time, so this effect must be due to relatively permanent surface changes taking place on the catalyst surface. NO_2 increase in the downstream products is likely due to oxidation of surface Pt–NO with Pt–O.

To investigate the surface change further, surface absorbance peaks were analyzed during thermal cycling of the catalyst under plasma exposure. Figures 8(a) and (b) compare the pattern for adsorbed NO and surface nitrate on both the catalyst and the support material.

In the first cycle for Pt–Al_2O_3, nitrate rises rapidly at the same position where NO_2 increases downstream in the second cycle (figure 4). Such an effect is not seen for the support material, where nitrate peaks rise steadily. For subsequent

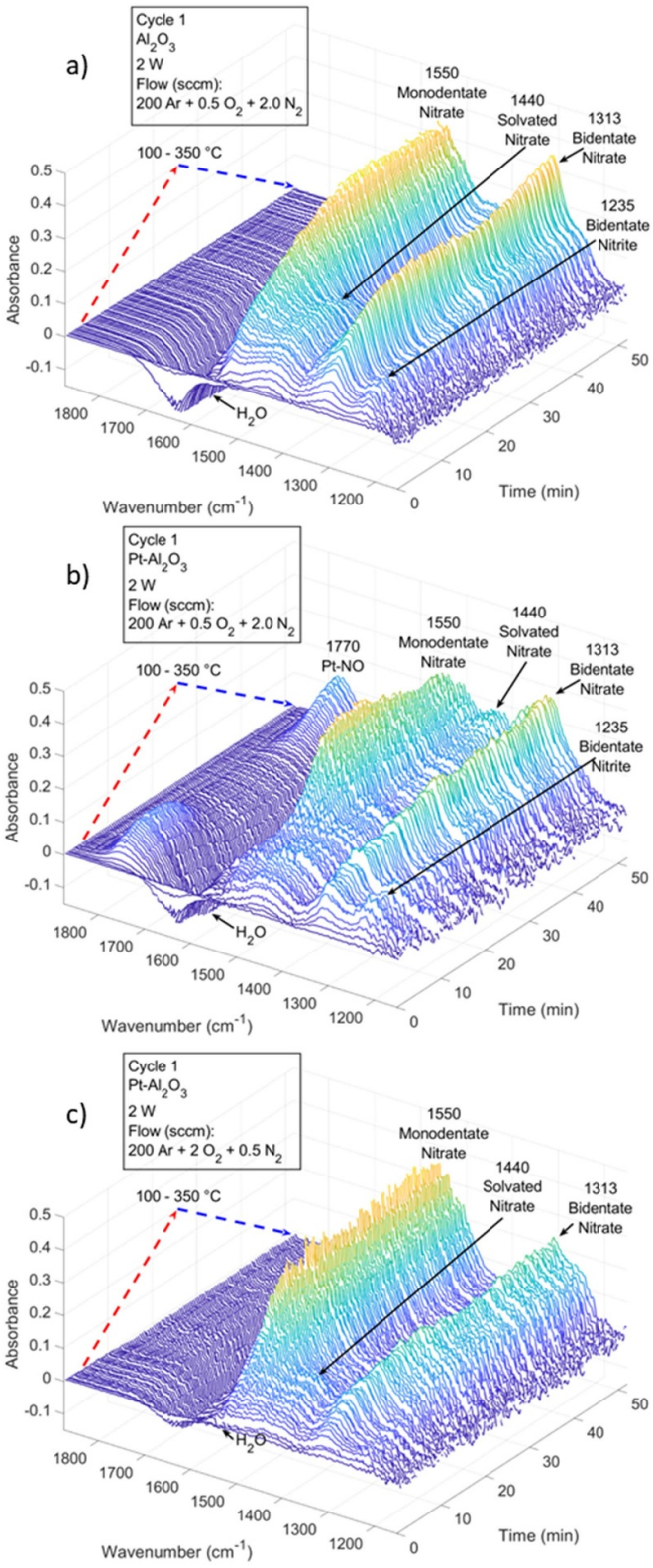

Figure 8. DRIFTS absorbance peaks during the first thermal cycle of Pt–Al_2O_3 or Al_2O_3 under 2 W plasma exposure. Background spectra were taken at 100 °C before the start of plasma exposure/cycling. Red arrow indicates heating, blue indicates cooling. Heating/cooling rate is 10 °C min^{-1} (a) Al_2O_3 N_2 rich. (b) Pt–Al_2O_3 N_2 rich. (c) Pt–Al_2O_3 O_2 rich.

cycles this nitrate effect does not occur on Pt–Al_2O_3. This may indicate that NO_x species hysteresis during the first cycle is suppressed by the formation of stable nitrates. Once these nitrate sites are occupied, products can leave into the gas phase. This explains the change in hysteresis pattern of downstream products during the first cycles (figures 4 and 5). This mechanism of spillover to nitrate sites is also supported in the literature [54, 75]. For the Al_2O_3 sample, there is no such correlation, as downstream patterns in all four cycles are consistent. Nitrates also build up steadily for O_2 rich plasma at 2 W (figure 8(c)) despite differences in product hysteresis over the first three cycles. This may be due to a greater flux of oxidants (O_3) to the surface which can oxidize Pt–NO on the top surface of the powder bed rapidly, even at low catalyst temperature.

O_3 production should increase with O_2/N_2 ratio at the same plasma power [42]. The buildup of nitrates is also faster for O_2 rich plasma than N_2 rich plasma, which is consistent with more oxidants being present in the incoming flux to the surface. For O_2 rich, 3.5 W plasma, which would result in a larger reactant flux to the surface, hysteresis curves become consistent one cycle faster, suggesting the speed of available nitrate site depletion is dependent on total flux to the surface.

Transient surface changes are demonstrated by the hysteresis loops themselves, with the production of NO and NO_2 showing strong substrate temperature dependence. These loops are likely caused by the buildup and depletion of reactants on the catalyst surface particularly Pt–NO and Pt–O, rather than a permanent change in NO_x production effectivity. Hysteresis loops are much more prominent for Pt–Al_2O_3 as opposed to Al_2O_3 which is due to Pt catalyzing the release of NO_x species absorbed on the Pt–Al_2O_3 catalyst, a known effect of Pt in NO_x adsorbing catalysts [54, 55]. Further analysis of the NO oxidation and NO_x desorption reactions taking place on the catalyst surface can be found in [38].

In effect there are two types of surface changes taking place. One is due to the buildup and depletion of reactants on the catalyst surface during thermal cycling and evidenced by hysteresis loops. The other is relatively permanent and is due to filling of certain sites on the support which may act as product sinks. Once this permanent change is completed, transient surface changes become repeatable.

4.2. *Influence of heating rate on plasma–catalyst interaction*

Changes in heating rate (figures 6 and 7) and power (figure 5) result in similar changes to NO and NO_2 heating curves, with more prominent hysteresis loops and an increase of downstream NO_2 and NO at a lower substrate temperature. This is consistent with the time-integrated reactant flux to the surface at low catalyst temperature being the primary driver of these features. With a lower heating rate, more total reactants will reach the surface at low temperatures. A lower heating rate also means more time at elevated temperature, which may contribute to the peak downstream density of NO_2 occurring for a lower temperature as the heating rate is lowered. When the heating rate is decreased, there is an increase in the time the catalyst is held at elevated temperatures, leading to an earlier occurrence of the NO_2 peak as a result of the depletion of available Pt–O for oxidation. The exact mechanism by which Pt–NO and Pt–O surface coverage lowers the temperature of product formation increase requires more investigation. Literature data indicates that oxygen (Pt–O) surface coverage can influence the bonding strength of NO. At high coverages, repulsive forces from Pt–O may lower the activation energy of both NO desorption and NO_2 formation [76, 77]. These surface dipole interactions may play a role in determining the temperature of product formation increase. The effect of total flux to the surface on NO_2 formation is clearly much stronger than the effect on NO desorption.

When the 3.5 W O_2 rich heating curves are plotted vs time as shown in figure 7, the measured downstream density of products begins to significantly increase at a similar time for each heating rate. This suggests that product formation is strongly influenced by surface coverage.

The cooling curves show a consistent pattern when plotted against catalyst temperature or time. This consistency may indicate that the reactants stored on the surface at low temperature have been depleted at this stage in the temperature cycle and both NO and NO_2 are descending to the steady state production values. Additionally, as the surface cools, it becomes less active for NO oxidation or desorption, leading to a return to low temperature surface interactions with reactants building up on the surface.

When examining the total NO_x produced, it is evident that the heating rate does not significantly alter the formation rate of the total product when a whole cycle is considered, with half the rate leading to double the product across one cycle. This finding is expected as the catalyst will spend double the time at both high and low temperatures. While prior work has shown that loss of NO_x may occur on the catalyst surface for N_2 rich conditions, this was not the case for O_2 rich conditions in later cycles. An overall efficiency increase in NO_x production due to the catalyst is also not seen in this and prior work [38]. This is also unsurprising for a few reasons. First, the catalyst temperature is too low for NO_x to form thermally [69]. Second, the convection timescales from nozzle to surface involved in this work are on the order of tens of milliseconds, which is likely longer than the lifetime of reactive species which may contribute to NO formation [71]. Pei *et al* have shown an improvement in energy efficiency of NO_x formation through plasma coupling with activated Al_2O_3, however a closer coupling of plasma and catalyst was required, and jet-like geometries were ineffective [24, 32].

The influence of heating rate on NO_2 formation can also be visualized by plotting NO_2 production versus NO production as shown in figure 9. As the heating rate decreases, the total amount of species delivered to the surface at low temperature increases. With a larger surface coverage of oxidative adsorbates, NO_2 production increases at the expense of NO. For O_2 rich conditions, the near vertical slope during initial heating for low heating rates indicates an almost complete oxidation of incoming and stored NO. As the catalyst cools, the slope moves closer to one, indicating that incoming O_2 and O_3 flux is required for NO oxidation as the adsorbate surface coverages formed initially have been depleted. For O_2 rich

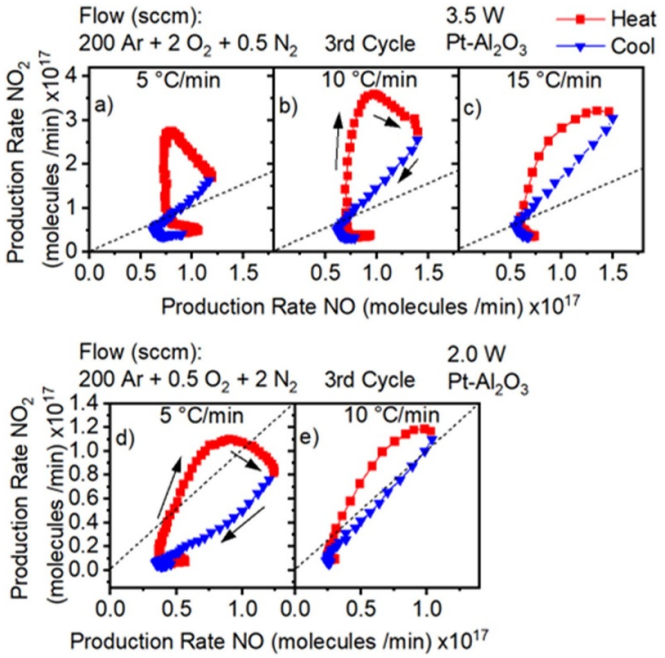

Figure 9. Comparison of NO_2 vs NO production during thermal cycling at different heating and cooling rates. NO_2 and NO become further decoupled as the rate decreases. Arrows indicate the thermal cycle path. (a) 5 °C min^{-1} O_2 rich. (b) 10 °C min^{-1} O_2 rich. (c) 15 °C min^{-1} O_2 rich. (d) 5 °C min^{-1} N_2 rich. (e) 10 °C min^{-1} N_2 rich.

conditions, decreasing the heating rate from 15 °C min^{-1} to 5 °C min^{-1} results in the increase in NO_x during heating to be entirely due to NO_2. This indicates that the activity for NO oxidation is greater than that of NO desorption at these temperatures and surface oxygen availability is the limiting factor for oxidation. The Pt–O is depleted before 350 °C resulting in a rise in NO, as incoming NO flux is deflected off the surface (not adsorbing on Pt or being oxidized by Pt–O) and causing the slope to become negative. For N_2 rich conditions, shown in figures 9(d) and (e), the shift in slope NO_2 vs NO slope with heating rate is not nearly as pronounced, however there is still an increase in overall hysteresis. A lower oxidizing flux to the surface at low catalyst temperature for N_2 rich plasma, and a higher ratio of Pt–NO to Pt–O on the surface, means that some Pt–NO adsorbed at low temperatures is not oxidized to NO_2 before desorbing. The dotted line in figures 9(a)–(e) indicates a 1:1 ratio of NO_2 to NO production. For O_2 rich conditions, O_2 rich conditions are heavily skewed towards NO_2 production, while N_2 rich are close to 1:1. This suggests that for N_2 rich conditions, NO production is not entirely due to deflection of incoming NO flux but from Pt–NO.

Figure 9 also suggests that the low temperature reactant coverage on the surface is metastable. When the surface is heated, these reactants combine rapidly to leave the surface. This effect is only enhanced with higher surface coverage of adsorbates, showing that increased coverage only lowers adsorbate stability.

4.2.1. Description of hysteresis. A hysteresis effect for NO oxidation with O_2 over Pt–Al_2O_3 catalyst has been seen by Hauff *et al* and Hauptmann *et al* when ramping between 150 °C and 400 °C [7, 78, 79]. As in our case, reverse hysteresis was observed, with NO_2 production during heating being larger than during cooling. However, there are numerous differences between the two observed patterns. In our case, the hysteresis in NO_2 production increases between cycle 1 and cycle 2 whereas it decreases in the work of Hauff *et al.* Additionally, the NO_2 production measured by Hauff *et al* is believed to be due to continuous oxidation of NO arriving at the surface, whereas we appear to see a storage and release of NO_x. We have previously shown that the steady state NO_x production in an empty reaction chamber is lower than the peak NO_x production during thermal cycling over Pt–Al_2O_3 but higher than the minimum for the same plasma conditions. As Pt is not expected to contribute significantly to NO_x production in this remote plasma set-up, this suggests a storage and release of NO_x species during thermal cycling. Also, for our conditions, if the plasma, and thus NO production, is turned off prior to a cycle, NO_2 and NO are still formed during thermal cycling due to metastable Pt–NO and Pt–O formed at low substrate temperature initially [38].

Hauff *et al* determined that the hysteresis mechanism centered on Pt oxidation that takes place at elevated temperatures by either O_2 or NO_2 product. Pt oxide is less active for NO oxidation than Pt metal, causing a decrease in NO oxidation rate after high temperature exposure. It was also seen that below 220 °C NO was able to partially reduce the Pt, allowing for an increased NO oxidation rate during the heating phase of the next cycle. This is a different mechanism than what we have described for the hysteresis seen with remote plasma-catalysis, where species build up on the surface at low temperature and subsequently react at high temperature. The differences between our conditions and those of Hauff *et al* may explain this discrepancy. In our case, fresh Pt catalyst is used, not pre-reduced catalyst, thus there may be some existing oxygen present on the surface at the beginning of the temperature cycle. Additionally, our flux to the surface at low temperature consists of not just O_2 and NO, but other plasma-produced species such as O_3. In such an environment, it is unlikely that the heating cycle begins with a reduced Pt surface, especially in O_2-rich conditions where the largest NO_2 hysteresis is seen.

It is possible that this change in activity of the Pt surface witnessed by Hauff *et al* is occurring at the same time as the metastable-derived product formation we witness. Figure 6 shows a larger hysteresis for lower heating rates, including lower NO_2 production at the same temperature during the cooling curves. It may be that the longer period of catalyst exposure at high temperatures results in decreased catalyst activity from Pt oxidation from the O_2 flux. This raises the question of what changes at low temperature to increase the catalyst activity for NO oxidation, which appears to be high during subsequent heating. It could be that oxygen formed on the catalyst by the plasma at low temperature is more mobile than that formed at high temperatures from O_2 flux, and more

readily reacts with NO to form NO_2. During cooling, the unreactive Pt oxide may be slowly reduced by NO flux and replaced by reactive oxygen adsorbed on Pt sites.

Here, for simplicity, it is assumed that the adsorption–desorption characteristics that take place during hysteresis are due to NO and O adsorption on the Pt surface. The actual mechanism may involve breakdown of surface nitrites/nitrates on the support, more description can be found in [38]. Oxidation of NO on Pt is thought to take place either through the Langmuir–Hinshelwood mechanism with adsorbed NO and O, or the Eley–Rideal mechanism with NO from the gas phase reacting with oxygen on the surface [50, 80, 81]. The reaction of metastable Pt–O and Pt–NO during heating clearly proceeds via the L–H mechanism. However, the lack of Pt–NO seen at high temperatures suggests that steady state NO_2 formed at high temperatures is due to incoming NO reacting directly with surface Pt–O, which may suggest an E–R mechanism. Here, oxidation of metastable Pt–NO is assumed to proceed through the L–H mechanism while steady state oxidation of NO at high temperatures is assumed to proceed through the E–R mechanism. Deactivation of Pt at high temperature through the formation of deactivating platinum oxide may also occur as described in the previous section. However, this does not appear to be the primary contributor to the hysteresis seen in this work and will thus be neglected in the reaction equations.

With these assumptions, we can create a basic model for the oxidation reaction. Restricting the model to either low or high catalyst temperature can help explain the experimentally observed hysteresis. Additionally, the model will help describe how the hysteresis pattern varies for O_2-rich and N_2-rich conditions. Starting with the relevant chemical reaction equations, shown below, formulas for Pt–NO and Pt–O surface coverage will be derived to show why these coverages rise and fall during the temperature ramp. Equations can also be developed for the measurable quantities of downstream gas-phase NO and NO_2 to evaluate if the observed metastability is consistent with the proposed reaction mechanism

$$\mathrm{NO} + \mathrm{Pt} \leftrightarrow \mathrm{Pt} - \mathrm{NO} \tag{4.1}$$

$$\mathrm{O_3} + \mathrm{Pt} \rightarrow \mathrm{Pt} - \mathrm{O} + \mathrm{O_2} \tag{4.2}$$

$$0.5\mathrm{O_2} + \mathrm{Pt} \rightarrow \mathrm{Pt} - \mathrm{O} \tag{4.3}$$

$$\mathrm{Pt} - \mathrm{NO} + \mathrm{Pt} - \mathrm{O} \rightarrow \mathrm{NO_2} + 2\mathrm{Pt} \tag{4.4}$$

$$\mathrm{NO} + \mathrm{Pt} - \mathrm{O} \leftrightarrow \mathrm{Pt} + \mathrm{NO_2}. \tag{4.5}$$

Equations (4.1) and (4.2), which increase Pt–O and Pt–NO surface coverage, are dependent on the plasma for production of NO and O_3, while equations (4.4) and (4.5), which decrease adsorbate surface coverage, will be more effected by the catalyst temperature, as will dissociation of O_2 (4.3). The site balance for Pt sites in this system can be written as below

$$n^* = n_\mathrm{s} - n_\mathrm{NO} - n_\mathrm{O} \tag{4.6}$$

where n represents the site densities, with n^* and n_s being the density of available Pt sites and the initially available Pt sites ($t = 0$), assumed to be the total number of sites, respectively, and n_NO and n_O being the sites occupied by NO and O respectively. By dividing this expression by the total number of sites n_s, equation (4.6) can be rewritten with the site coverage fractions θ where $\theta^* = \frac{n^*}{n_\mathrm{s}}$. The initial Pt site coverage fraction is 1, yielding equation (4.7) below

$$\theta^* = 1 - \theta_\mathrm{NO} - \theta_\mathrm{O}. \tag{4.7}$$

The change in surface coverage fractions of Pt–NO and Pt–O can be approximated by a flux balance of the respective compounds adsorption or removal from the surface, via desorption or reaction. From (4.1) and (4.4) we obtain the below equation for the formation rate of Pt–NO

$$\frac{\mathrm{d}\theta_\mathrm{NO}}{\mathrm{d}t} = \frac{s_\mathrm{NO}(\theta,T)\,\Gamma_\mathrm{NO}\theta^*}{n_\mathrm{s}} - \nu_\mathrm{NO}\theta_\mathrm{NO}\mathrm{e}^{\frac{Ea_\mathrm{NO}}{kT}} - \theta_\mathrm{NO}\theta_\mathrm{O}\nu_\mathrm{L}\mathrm{e}^{\frac{Ea_\mathrm{L}}{kT}} \tag{4.8}$$

where $s_\mathrm{NO}(\theta,T)$ is the sticking probability of NO on Pt, Γ_NO is the flux of plasma produced NO to the catalyst surface, ν_NO is the vibrational frequency of NO, ν_L is the frequency that determines the Pt–NO and Pt–O interaction. Ea_NO is the activation energy for thermal desorption of NO from the Pt surface while Ea_L is the activation energy for NO_2 formation via the Langmuir–Hinshelwood mechanism. This equation ignores the activation energies for NO adsorption on Pt, which is very low [82]. The sticking probability is dependent on both existing adsorbate surface coverage, where it decreases with fewer open Pt sites, and surface temperature and thus will vary with time. For low substrate temperatures, Pt–NO coverage will be dependent on adsorption of incoming NO flux and will rise until a steady-state is reached. At high substrate temperatures, loss terms of Pt–NO will dominate, resulting in a low NO surface coverage. Additionally, the higher the Pt–O coverage, the more the third term for NO_2 formation will increase in expense of the second for NO desorption. It may be possible in plasma–catalyst situations to have another mechanism of NO loss via direct oxidation by ROS species O or O_3. The likelihood of this interaction will depend not just on ROS flux and Pt–NO coverage but also plasma–catalyst proximity in the case of O, which has a very short lifetime in the gas phase compared to NO [71]. For the purposes of this model, for our remote-plasma catalyst configuration, these reactions are not considered.

From reactions (4.2)–(4.5) we can obtain an equation for Pt–O formation

$$\frac{\mathrm{d}\theta_O}{\mathrm{d}t} = \frac{s_{\mathrm{O_3}}(\theta,T)\,\Gamma_{\mathrm{O_3}}\theta^*}{n_\mathrm{s}} + 2\frac{s_{\mathrm{O_2}}(\theta,T)\,\Gamma_{\mathrm{O_2}}\theta^*\mathrm{e}^{\frac{Ea_\mathrm{d}}{kT}}}{n_\mathrm{s}} - \theta_\mathrm{NO}\theta_\mathrm{O}\nu_\mathrm{L}\mathrm{e}^{\frac{Ea_\mathrm{L}}{kT}} - \frac{\Gamma_\mathrm{NO}\theta_\mathrm{O}k}{n_\mathrm{s}} \tag{4.9}$$

Ea_d is the activation energy of O_2 desorption, and k is the probability of the gas-phase NO reacting with Pt–O. O_2 Associative desorption of O_2 is not present in the equation as it does not typically occur below 400 °C and thus is not considered [50]. Dissociation of O_2 results in two Pt–O sites,

while for simplicity, it is assumed that the interaction of O_3 with the surface results in one Pt–O and the resulting O_2 escapes. O_3 is known to be highly reactive with Pt surfaces and will quickly decompose at catalyst temperatures as low as 70 °C, thus the activation energy of O_3 dissociation on Pt is not considered here [83]. It can be seen that as the temperature is ramped, Pt–O formation will be driven more and more by O_2 dissociation. At low substrate temperatures, the Pt–O formation will dominate over loss and Pt–O surface coverage will be primarily dependent on incoming O_3. At high substrate temperatures, Pt–O coverage will depend on the balance between NO_2 formation (terms 3 and 4) and O_2 dissociation.

The change in surface coverage of Pt–NO and Pt–O between low and high catalyst temperature is what defines the metastability, as the loss rates are driven by NO and NO_2 formation. Because the loss rates increase with adsorbate surface coverage, adsorption of Pt–O and Pt–NO at the beginning of the temperature ramp results in a spike in NO and NO_2 evolving from the surface, which is the hysteresis seen in the data.

While Pt–NO can be measured with DRIFTS for N_2-rich conditions, Pt–O and the empty site fraction cannot. To further evaluate this system, we can construct equations based on downstream gas-phase NO and NO_2, which are measurable. From equation (4.1) through (4.5) we can see that the measured gas phase NO downstream of the reaction is dependent on the incoming flux to the catalyst, loss to the surface ((4.1) and (4.5)), and gain from the surface (4.1). Change in downstream NO_2, assuming a stable flux produced by the plasma, is purely dependent on gain from the catalyst surface ((4.4) and (4.5)). The equation for downstream gas-phase NO, Γ^{g}_{NO}, can be formulated below

$$\Gamma^{G}_{NO} \propto \overbrace{\Gamma_{NO}}^{a} - \overbrace{\Gamma_{NO} s_{NO}(\theta,T)\theta^{*}}^{b} - \overbrace{\Gamma_{NO}\theta_{O}\nu_{E}k}^{c} + \overbrace{n_{s}\nu_{NO}\theta_{NO}e^{\frac{Ea_{NO}}{kT}}}^{d} \tag{4.10}$$

where term *a* shows the flux of NO to the catalyst surface, term *b* shows the loss of NO to adsorption on Pt, term *c* shows loss of NO to reaction with surface Pt–O, and term *d* shows gain of NO from desorption from the Pt surface. The equation for NO_2 is shown in a similar way below

$$\Gamma^{G}_{NO_2} \propto \overbrace{\Gamma_{NO_2}}^{a} + \overbrace{\Gamma_{NO}\theta_{O}k}^{b} + \overbrace{n_{s}\theta_{NO}\theta_{O}\nu_{L}e^{\frac{Ea_{L}}{kT}}}^{c} \tag{4.11}$$

where term *a* shows NO_2 produced in the plasma, term *b* shows the formation of NO_2 from incoming NO and Pt–O, and term *c* shows the formation of NO_2 via the reaction of surface Pt–NO and Pt–O.

We can see that the formation rate of NO_2 increases with Pt–O coverage while the NO rate decreases. We also find that NO_2 formation, and NO desorption rates increase with substrate temperature. If the reactant flux to the surface is constant, then the steady-state Pt–O and Pt–NO surface coverage will be lower at high substrate temperature than at low substrate temperature. Temperature programmed desorption shows that the majority of low temperature adsorbed NO on Pt–Al_2O_3 is thought to desorb once a substrate temperature of 350 °C has been reached [84]. This shift from high to low coverage upon raising the catalyst temperature would result in release or oxidation of NO, resulting in hysteresis.

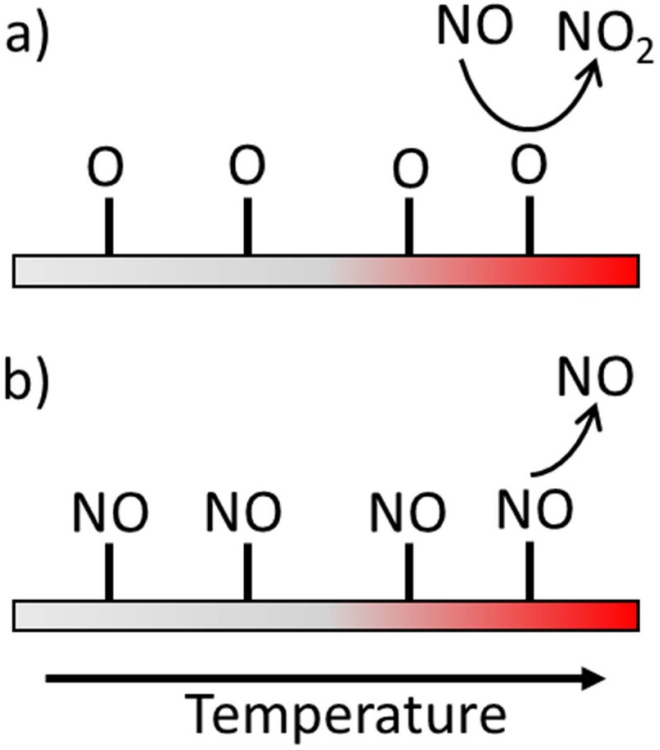

Figure 10. (a) Depiction of hysteresis effect for conditions with $O_2 \gg N_2$ in the plasma feed gas. (b) Depiction of hysteresis effect for conditions with $N_2 \gg O_2$ in the plasma feed gas. Low temperature conditions on the left depict the metastable adsorbate makeup, high temperature conditions on the right show the formed product.

For very O_2 rich conditions, the low temperature fractional surface coverage is likely dominated by Pt–O with $\theta_O \gg \theta_{NO}$. Thus, the last terms of equations (4.10) and (4.11) can be ignored and the formation rate of NO_2 during hysteresis is driven by oxidation of incoming NO flux, depicted in figure 10(a). As Pt–O coverage drops, NO_2 production rate will also drop, while NO downstream will increase as less of it is being oxidized. For extreme N_2 rich conditions, low temperature adsorbate surface coverage is likely dominated by Pt–NO with $\theta_{NO} \gg \theta_O$. In these cases, NO_2 formation is minimal, and hysteresis is formed from NO desorbing from the surface, depicted in figure 10(b). Our conditions exist between these two extremes, with $\theta_O > \theta_{NO}$ or $\theta_{NO} > \theta_O$. In these cases, oxidation of metastable Pt–NO by Pt–O also contributes to the hysteresis.

4.3. General description of plasma–catalyst interaction

Cold atmospheric pressure plasma (CAPP) is distinguished by its unique non-equilibrium characteristics. Unlike thermal plasmas, where temperatures are uniform across electrons, ions, and neutrals, CAPP exhibits a significant disparity,

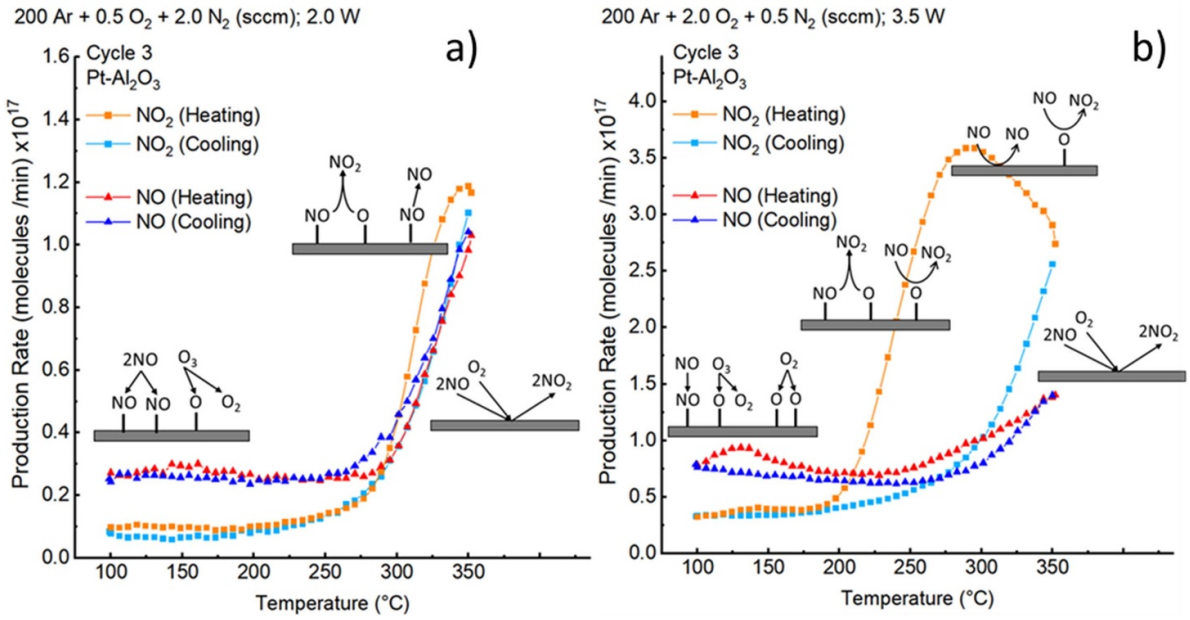

Figure 11. Descriptive drawing of plasma catalyst interaction. (a) N_2 rich. Metastable Pt–NO and Pt–O form at low temperature with Pt–NO > Pt–O. As the temperature is ramped, metastable adsorbates react to form NO_2 or desorb as NO. Subsequent plasma exposure results in a steady state system of species arriving at the catalyst surface and quickly reacting. (b) Metastable Pt–NO and Pt–O form at low temperature with Pt–O > Pt–NO. As the temperature is ramped, incoming NO is oxidized to NO_2 and metastable adsorbates react to form NO_2. As Pt–O is depleted, NO is deflected off the Pt surface. Subsequent plasma exposure results in a steady state system of species arriving at the catalyst surface and quickly reacting.

primarily between the electron temperature and the much cooler heavy species (ions and neutrals). This non-equilibrium state allows for high electron energies that facilitate various chemical reactions without substantially increasing the overall gas temperature. Electron impact excitation, vibrational-vibrational energy transfer, or vibrational-electronic energy transfer are just some ways in which gas molecules within the plasma may have their bonds weakened or broken, greatly increasing the reactivity of these species. When the plasma interfaces with a catalyst surface, the non-equilibrium nature of the plasma may impart a metastable characteristic to the catalyst surface. This may be due to deposition of atomic species [85], surface charging which may change the adsorption characteristics of the surface [86–88], or other morphology changes. We refer to these changes as metastable as they may cease post plasma-application or upon the introduction of another reactant gas stream. An underexplored aspect of these metastable surfaces is how they change upon heating. Elevated temperature is often employed in standard catalytic reactions, as the decrease in activation energy from the catalyst alone is not sufficient for the desired reaction. Additionally, adsorption and desorption properties of the catalyst may be affected by the catalyst temperature.

In the case of plasma catalysis, elevating catalyst temperature may induce reactions on the metastable surface. In our case, heating the catalyst likely induced a reaction of surface adsorbed NO and oxygen to form NO_2. Heating past a certain point may also result in desorption of adsorbed NO, which can be seen in the hysteresis curves of figure 4. Initially, a non-equilibrium flux at low temperatures from the plasma results in a metastable surface coverage of RONS and oxygen which would not otherwise form. Heating to high temperatures leads to a reduction in this surface coverage, followed by a steady-state reaction of incoming reactive species. The cycle then repeats with a return to low temperatures, leading to the re-establishment of non-equilibrium surface coverage. The metastable surface coverage is clearly sensitive to plasma parameters such as feed gas and power, but also exposure time. Figure 6(a) shows that increased exposure time changes the temperature of NO_2 product increase drastically. Certain reaction features may be affected differently by degree of coverage. For instance, figure 6(b) shows that changes to adsorbate surface coverage have little effect on the hysteresis loop of NO desorption. In our work, the separation between plasma and catalyst causes the primary incident reactive species to be long lived RONS or ROS. With a closer plasma catalyst coupling, shorter lived reactive species may also impinge on the surface such as atomic nitrogen. A colder surface may be required to prevent these species from recombining. Thus, there are a plethora of ways to tune the adsorbate surface coverage at low temperature.

Figure 11 depicts schematically the plasma–catalyst interaction in this system and may be applicable to plasma–catalytic systems generally. The non-equilibrium characteristic of the plasma results in an unstable surface coverage that can only exist at low temperatures. In our system this is likely due to a coverage of Pt–NO and Pt–O formed from plasma produced gas species. As the catalyst is heated, these adsorbates react to form NO_2. When the metastable surface coverage is depleted from high temperature reactions, downstream products are governed by steady state reactions of fluxes arriving at the catalyst surface. For N_2 rich feed-gas,

figure 11(a), the primary cause of NO_2 and NO hysteresis is the Pt–NO and Pt–O reaction and Pt–NO desorption respectively. For O_2 rich feed-gas, figure 11(b), the high Pt–O surface coverage results in NO_2 hysteresis being driven primarily by oxidation of inbound NO as well as oxidation of Pt–NO. In this case, NO hysteresis likely results from inbound NO no longer being adsorbed on the catalyst surface or oxidized to NO_2.

In this way, the knowledge gained from this work may be helpful for the design of plasma-catalysis generally. The tailoring of desired surface adsorbates can be achieved with a cold plasma, where the cold surface allows for a metastable surface coverage. Subsequently heating the catalyst to a desired temperature can then induce surface reactions to form desired gas species. Understanding plasma catalysis in this manner may, with variable catalyst temperature, increase the mechanisms by which reactions can be optimized.

5. Conclusion

In this work, the interaction of an $Ar/N_2/O_2$ cold atmospheric-pressure plasma jet with a Pt–Al_2O_3 catalyst was studied with IR based techniques. The catalyst temperature was cycled during plasma exposure to understand the effect catalyst temperature has on the interaction. Thermal cycling under plasma exposure revealed hysteresis in NO_x production, primarily NO_2, resulting in a large increase in production as the temperature is elevated. This was attributed to adsorption of reactants at low temperatures and their subsequent reaction and release at high temperatures. Correlation of downstream products and surface species revealed that long-lasting changes take place during the first cycles, due to the stabilization of the surface and the filling of certain sites on the Al_2O_3 support. The degree of hysteresis is influenced by the total flux to the surface at low temperature and the build-up of Pt–O. Thus, lowering the thermal cycle ramp rate has a similar effect on hysteresis as increasing the instantaneous reactant flux. This is evident from the observation that NO_2 rises at lower temperatures and increases rapidly relative to NO. Lastly, the earlier depletion of Pt–O reduces the effectiveness of oxidation at high temperatures. This suggests that at higher substrate temperatures, oxidation becomes dependent on the incoming O_2 flux, highlighting the importance of flux and temperature in determining surface reactions and product formation.

The overall reaction can be described by the formation of a metastable surface coverage due to plasma exposure at low temperature where surface reactivity is low. Subsequently, ramping the catalyst temperature increases adsorbate reactivity and results in the formation of species which desorb into the gas phase. The effect of varying catalyst temperature is under-studied in the field of plasma catalysis. At conditions with low surface reactivity, plasma catalyst interaction can be controlled to yield a desired adsorbate surface coverage which may not react until the catalyst temperature is elevated. Compared to conditions where reactants adsorb on the surface and react instantly, an approach of variable catalyst temperature may allow for greater selectivity. Hopefully, the application of this approach to a variety of plasma–catalytic systems in the future can produce valuable insights on plasma–catalyst mechanisms.

Data availability statement

The data cannot be made publicly available upon publication because they are not available in a format that is sufficiently accessible or reusable by other researchers. The data that support the findings of this study are available upon reasonable request from the authors.

Acknowledgment

This material is based upon work supported by the U.S. Department of Energy, Office of Science, Office of Fusion Energy Sciences under Award Number DE-SC0020232. We thank Dr Peter Bruggeman, Dr Aditya Bhan, Brian Bayer, Audrey Fehlhaber, Yudong Li, Dr Shiqiang Zhang, and Sang-Jin Chung for helpful discussions and contributions to this work.

ORCID iDs

Michael Hinshelwood https://orcid.org/0009-0008-5808-8830
Gottlieb S Oehrlein https://orcid.org/0000-0002-6693-4274

References

[1] Yamaguchi M 2024 Thermal hysteresis involving reversible self-catalytic reactions *Acc. Chem. Res.* **54** 2603–13
[2] Dusch Y, Rudenko V, Tiercelin N, Giordano S and Preobrazhensky V 2012 Hysteretic magnetoresistance in stress controlled magnetic memory device *Nanomater. Nanostruct.* **2** 44–50
[3] Damjanovic D 2006 Hysteresis in piezoelectric and ferroelectric materials *The Science of Hysteresis* vol 3 (Elsevier) pp 337–465
[4] Ball P C and Evans R 2024 Temperature dependence of gas adsorption on a mesoporous solid: capillary criticality and hysteresis *Langmuir* **5** 714–23
[5] Puibasset J 2010 Counting metastable states within the adsorption/desorption hysteresis loop: a molecular simulation study of confinement in heterogeneous pores *J. Chem. Phys.* **133** 104701
[6] Subbotin A N, Gudkov B S and Yakerson V I 2000 Temperature hysteresis phenomena in heterogeneous catalysis *Russ. Chem. Bull.* **49** 1373–9
[7] Hauptmann W, Votsmeier M, Gieshoff J, Drochner A and Vogel H 2009 Inverse hysteresis during the NO oxidation on Pt under lean conditions *Appl. Catal.* B **93** 22–29
[8] Casapu M, Fischer A, Gänzler A M, Popescu R, Crone M, Gerthsen D, Türk M and Grunwaldt J-D 2017 Origin of the normal and inverse hysteresis behavior during CO oxidation over Pt/Al_2O_3 *ACS Catal.* **7** 343–55
[9] Al Soubaihi R M, Saoud K M and Dutta J 2018 Critical review of low-temperature CO oxidation and hysteresis phenomenon on heterogeneous catalysts *Catalysts* **8** 660
[10] Pakharukov I, Prosvirin I P, Chetyrin I A, Bukhtiyarov V I and Parmon V N 2016 *In situ* XPS studies of kinetic hysteresis

in methane oxidation over Pt/γ-Al_2O_3 catalysts *Catal. Today* **278** 135–9
[11] Everett D H and Whitton W I 1952 A general approach to hysteresis *Trans. Faraday Soc.* **48** 749–57
[12] Wang S, Cai W, Li J, Wei W and Hu J 2013 A novel rapid D.C. plasma nitriding at low gas pressure for 304 austenitic stainless steel *Mater. Lett.* **105** 47–49
[13] DeVries R C 2024 Synthesis of diamond under metastable conditions *Annu. Rev. Mater. Sci.* **17** 161–87
[14] Baranovski S 2006 *Charge Transport in Disordered Solids with Applications in Electronics* (John Wiley & Sons) p 500
[15] Mohammed M A, Stabile R, Melskens J, Kessels W M M and Raz O 2018 Metastable hydrogenated amorphous silicon (a-Si:H) as reversible programmable photonic material: 2018 *MRS Fall Meeting & Exhibit*
[16] Winter L R, Ashford B, Hong J, Murphy A B and Chen J G 2020 Identifying surface reaction intermediates in plasma catalytic ammonia synthesis *ACS Catal.* **10** 14763–74
[17] Whitehead J C 2016 Plasma–catalysis: the known knowns, the known unknowns and the unknown unknowns *J. Phys. D: Appl. Phys.* **49** 243001
[18] Tendero C, Tixier C, Tristant P, Desmaison J and Leprince P 2006 Atmospheric pressure plasmas: a review *Spectrochim. Acta* B **61** 2–30
[19] Keidar M, Weltmann K D and Macheret S 2021 Fundamentals and applications of atmospheric pressure plasmas *J. Appl. Phys.* **130** 080401
[20] Neyts E C, Ostrikov K, Sunkara M K and Bogaerts A 2015 Plasma catalysis: synergistic effects at the nanoscale *Chem. Rev.* **115** 13408–46
[21] Wang Z, Zhang Y, Neyts E C, Cao X, Zhang X, Jang B W L and Liu C-J 2018 Catalyst preparation with plasmas: how does it work? *ACS Catal.* **8** 2093–110
[22] Li Y, Hinshelwood M and Oehrlein G S 2022 Investigation of Ni catalyst activation during plasma-assisted methane oxidation *J. Appl. Phys.* **55** 155202
[23] Li Y, Jiang J, Hinshelwood M, Zhang S, Bruggeman P J and Oehrlein G S 2022 Characterization of plasma catalytic decomposition of methane: role of atomic O and reaction mechanism *J. Appl. Phys.* **55** 155204
[24] Pei X *et al* 2024 Nitrogen fixation as NO_x using air plasma coupled with heterogeneous catalysis at atmospheric pressure *Plasma Process. Polym.* **21** 2300135
[25] Bouchoul N, Touati H, Fourré E, Clacens J M and Batiot-Dupeyrat C 2021 Efficient plasma-catalysis coupling for CH_4 and CO_2 transformation in a fluidized bed reactor: comparison with a fixed bed reactor *Fuel* **288** 119575
[26] Nozaki T and Okazaki K 2013 Non-thermal plasma catalysis of methane: principles, energy efficiency, and applications *Catal. Today* **211** 29–38
[27] Wang Y, Craven M, Yu X, Ding J, Bryant P, Huang J and Tu X 2019 Plasma-enhanced catalytic synthesis of ammonia over a Ni/Al_2O_3 catalyst at near-room temperature: insights into the importance of the catalyst surface on the reaction mechanism *ACS Catal.* **9** 10780–93
[28] Cherkasov N, Ibhadon A O and Fitzpatrick P 2015 A review of the existing and alternative methods for greener nitrogen fixation *Chem. Eng. Process.* **90** 24–33
[29] Shi R, Zhang X, Waterhouse G I N, Zhao Y and Zhang T 2020 The journey toward low temperature, low pressure catalytic nitrogen fixation *Adv. Energy Mater.* **10** 2000659
[30] Rouwenhorst K H, Jardali F, Bogaerts A and Lefferts L 2021 From the Birkeland–Eyde process towards energy-efficient plasma-based NO_X synthesis: a techno-economic analysis *Energy Environ. Sci.* **14** 2520–34
[31] Vervloessem E, Aghaei M, Jardali F, Hafezkhiabani N and Bogaerts A 2020 Plasma-based N_2 fixation into NO_x: insights from modeling toward optimum yields and energy costs in a gliding arc plasmatron *ACS Sustain. Chem. Eng.* **8** 9711–20
[32] Pei X, Gidon D and Graves D B 2019 Specific energy cost for nitrogen fixation as NO_x using DC glow discharge in air *J. Phys. D: Appl. Phys.* **53** 044002
[33] Ma H, Sharma R K, Welzel S, van de Sanden M C M, Tsampas M N and Schneider W F 2022 Observation and rationalization of nitrogen oxidation enabled only by coupled plasma and catalyst *Nat. Commun.* **13** 402
[34] Patil B S, Cherkasov N, Lang J, Ibhadon A O, Hessel V and Wang Q 2016 Low temperature plasma-catalytic NO_x synthesis in a packed DBD reactor: effect of support materials and supported active metal oxides *Appl. Catal.* B **194** 123–33
[35] Zhang S and Oehrlein G S 2021 From thermal catalysis to plasma catalysis: a review of surface processes and their characterizations *J. Appl. Phys.* **54** 213001
[36] Bligaard T, Nørskov J K and Lundqvist B I 2008 Understanding heterogeneous catalysis from the fundamentals *Handbook of Surface Science* vol 3, ed E Hasselbrink and B I Lundqvist (Elsevier) pp 269–340
[37] Védrine J C 2018 Fundamentals of heterogeneous catalysis *Metal Oxides in Heterogeneous Catalysis* (*Metal Oxides*) ed J C Védrine (Elsevier) ch 1, pp 1–41 (available at: www.sciencedirect.com/science/article/pii/B9780128116319000016)
[38] Hinshelwood M and Oehrlein G S 2023 Plasma catalysis: separating plasma and surface contributions for an Ar/N_2/O_2 atmospheric discharge interacting with a Pt catalyst *Plasma Sources Sci. Technol.* **32** 125001
[39] Knoll A J, Zhang S, Lai M, Luan P and Oehrlein G S 2019 Infrared studies of gas phase and surface processes of the enhancement of catalytic methane decomposition by low temperature plasma *J. Phys. D: Appl. Phys.* **52** 225201
[40] Zhang S, Sobota A, van Veldhuizen E M and Bruggeman P J 2015 Temporally resolved ozone distribution of a time modulated RF atmospheric pressure argon plasma jet: flow, chemical reaction, and transient vortex *Plasma Sources Sci. Technol.* **24** 045015
[41] Hofmann S, van Gessel A F H, Verreycken T and Bruggeman P 2011 Power dissipation, gas temperatures and electron densities of cold atmospheric pressure helium and argon RF plasma jets *Plasma Sources Sci. Technol.* **20** 065010
[42] Gaens W V, Bruggeman P J and Bogaerts A 2014 Numerical analysis of the NO and O generation mechanism in a needle-type plasma jet *New J. Phys.* **16** 063054
[43] Chen X, Huo X, Liu J, Wang Y, Werth C J and Strathmann T J 2017 Exploring beyond palladium: catalytic reduction of aqueous oxyanion pollutants with alternative platinum group metals and new mechanistic implications *Chem. Eng. J.* **313** 745–52
[44] Engelbrecht N, Chiuta S and Bessarabov D G 2018 A highly efficient autothermal microchannel reactor for ammonia decomposition: analysis of hydrogen production in transient and steady-state regimes *J. Power Sources* **386** 47–55
[45] Gordon I E *et al* 2017 The HITRAN2016 molecular spectroscopic database *J. Quant. Spectrosc. Radiat. Transf.* **203** 3–69
[46] Bartlett R W 1967 Platinum oxidation kinetics with convective diffusion and surface reaction *J. Electrochem. Soc.* **114** 547
[47] Johnson Matthey Technology Review *The Oxidation of the Platinum Metals* (available at: www.technology.matthey.com/article/19/4/135-140/) (Accessed 11 October 2021)
[48] Plessow P N and Abild-Pedersen F 2016 Sintering of Pt nanoparticles via volatile PtO_2: simulation and comparison with experiments *ACS Catal.* **6** 7098–108
[49] Yeo C D, He M, Lee J, Shah N M R, Hong Y K, Choi M, You J H, Purani D and Lee J K 2020 Recovering magnetic

domains of nanoscale-mechanically damaged ferromagnetic thin film of information data storage *Appl. Mater. Today* **21** 100825
[50] Olsson L, Westerberg B, Persson H, Fridell E, Skoglundh M and Andersson B 1999 A kinetic study of oxygen adsorption/desorption and NO oxidation over Pt/Al_2O_3 catalysts *J. Phys. Chem.* B **103** 10433–9
[51] Wright A M, Sun C and Dincă M 2021 Thermal cycling of a MOF-based NO disproportionation catalyst *J. Am. Chem. Soc.* **143** 681–6
[52] Gholami R, Stere C E, Goguet A and Hardacre C 2018 Non-thermal-plasma-activated de-NO_x catalysis *Phil. Trans. R. Soc.* A **376** 20170054
[53] Hoard J 2001 Plasma-catalysis during temperature transient testing *Report No.: CONF-2000108-83* (Ford Research Laboratory (US)) (available at: www.osti.gov/biblio/827982) (Accessed 1 January 2024)
[54] Castoldi L, Matarrese R, Morandi S, Righini L and Lietti L 2018 New insights on the adsorption, thermal decomposition and reduction of NO_x over Pt- and Ba-based catalysts *Appl. Catal.* B **224** 249–63
[55] Castoldi L, Righini L, Matarrese R, Lietti L and Forzatti P 2015 Mechanistic aspects of the release and the reduction of NO_x stored on $Pt–Ba/Al_2O_3$ *J. Catal.* **328** 270–9
[56] Toops T J, Smith D B, Epling W S, Parks J E and Partridge W P 2005 Quantified NO_x adsorption on Pt/K/gamma-Al_2O_3 and the effects of CO_2 and H_2O *Appl. Catal.* B **58** 255–64
[57] Yu Y, He H, Feng Q, Gao H and Yang X 2004 Mechanism of the selective catalytic reduction of NO_x by C_2H_5OH over Ag/Al_2O_3 *Appl. Catal.* B **49** 159–71
[58] Yu S, Niu X, Song Z, Huang X, Peng Y and Li J 2022 Improvement of Al_2O_3 on the multi-pollutant control performance of NO_x and chlorobenzene in vanadia-based catalysts *Chemosphere* **289** 133156
[59] Toops T J, Smith D B and Partridge W P 2005 Quantification of the *in situ* DRIFT spectra of Pt/K/γ-$A1_2O_3$ NO_x adsorber catalysts *Appl. Catal.* B **58** 245–54
[60] Ji Y, Bai S and Crocker M 2015 Al_2O_3-based passive NO_x adsorbers for low temperature applications *Appl. Catal.* B **170–171** 283–92
[61] Narula C K, Allard L F, Stocks G M and Moses-debusk M 2014 Remarkable NO oxidation on single supported platinum atoms *Sci. Rep.* **4** 7238
[62] Wang C, Kong L, Jin S, Xia L, Tan J and Wang Y 2022 Effect of diesel soot on the heterogeneous reaction of NO_2 on the surface of γ-Al_2O_3 *Atmosphere* **13** 333
[63] Baltrusaitis J, Schuttlefield J, Jensen J H and Grassian V H 2007 FTIR spectroscopy combined with quantum chemical calculations to investigate adsorbed nitrate on aluminium oxide surfaces in the presence and absence of co-adsorbed water *Phys. Chem. Chem. Phys.* **9** 4970–80
[64] Nova I *et al* 2004 NO_x adsorption study over Pt–Ba/alumina catalysts: FT-IR and pulse experiments *J. Catal.* **222** 377–88
[65] Du C, Kong L, Zhanzakova A, Tong S, Yang X, Wang L, Fu H, Cheng T, Chen J and Zhang S 2018 Impact of heterogeneous uptake of nitrogen dioxide on the conversion of acetaldehyde on gamma-alumina in the absence and presence of simulated solar irradiation *Atmos. Environ.* **187** 282–91
[66] Wakabayashi R, Tomita A and Kimura T 2020 Understanding of NO_x storage property of impregnated Ba species after crystallization of mesoporous alumina powders *J. Hazard. Mater.* **398** 122791
[67] Ottinger N A, Toops T J, Nguyen K, Bunting B G and Howe J 2011 Effect of lean/rich high temperature aging on NO oxidation and NO_x storage/release of a fully formulated lean NO_x trap *Appl. Catal.* B **101** 486–94
[68] Pieta I S, García-Diéguez M, Herrera C, Larrubia M A and Alemany L J 2010 *In situ* DRIFT–TRM study of simultaneous NO_x and soot removal over Pt–Ba and Pt–K NSR catalysts *J. Catal.* **270** 256–67
[69] Ma Q, Liu Y and He H 2008 Synergistic effect between NO_2 and SO_2 in their adsorption and reaction on γ-alumina *J. Phys. Chem.* A **112** 6630–5
[70] Sedlmair C, Seshan K, Jentys A and Lercher J A 2003 Elementary steps of NO_x adsorption and surface reaction on a commercial storage–reduction catalyst *J. Catal.* **214** 308–16
[71] van Gessel A F H, Alards K M J and Bruggeman P J 2013 NO production in an RF plasma jet at atmospheric pressure *J. Phys. D: Appl. Phys.* **46** 265202
[72] Gaens W V and Bogaerts A 2013 Kinetic modelling for an atmospheric pressure argon plasma jet in humid air *J. Phys. D: Appl. Phys.* **46** 275201
[73] Schmidt-Bleker A, Bansemer R, Reuter S and Weltmann K D 2016 How to produce an NO_x-instead of O_x-based chemistry with a cold atmospheric plasma jet *Plasma Process. Polym.* **13** 1120–7
[74] Shimizu T, Sakiyama Y, Graves D B, Zimmermann J L and Morfill G E 2012 The dynamics of ozone generation and mode transition in air surface micro-discharge plasma at atmospheric pressure *New J. Phys.* **14** 103028
[75] Gao B, Zhang N, Zhang H, Qiu R, Chen Z, Li Y and Yang Z 2022 Effects of platinum high-temperature redispersion on Pt/Al_2O_3 diesel oxidation catalyst for nitric oxide oxidation and its reaction pathway *J. Environ. Chem. Eng.* **10** 108669
[76] Crocoll M, Kureti S and Weisweiler W 2005 Mean field modeling of NO oxidation over Pt/Al_2O_3 catalyst under oxygen-rich conditions *J. Catal.* **229** 480–9
[77] Getman R B and Schneider W F 2010 DFT-based coverage-dependent model of Pt-catalyzed NO oxidation *ChemCatChem* **2** 1450–60
[78] Hauff K, Tuttlies U, Eigenberger G and Nieken U 2012 Platinum oxide formation and reduction during NO oxidation on a diesel oxidation catalyst—experimental results *Appl. Catal.* B **123–124** 107–16
[79] Hauff K, Dubbe H, Tuttlies U, Eigenberger G and Nieken U 2013 Platinum oxide formation and reduction during NO oxidation on a diesel oxidation catalyst—macrokinetic simulation *Appl. Catal.* B **129** 273–81
[80] Wan S, Keller K, Lott P, Bhimrao Shirsath A, Tischer S, Häber T, Suntz R and Deutschmann O 2022 Experimental and numerical investigation of NO oxidation on Pt/Al_2O_3—and NO_x storage on $Pt/BaO/Al_2O_3$-catalysts *Catal. Sci. Technol.* **12** 4456–70
[81] Arevalo R L, Escaño M C S and Kasai H 2015 First-principles study of nitric oxide oxidation on Pt(111) versus Pt overlayer on 3D transition metals *J. Vac. Sci. Technol.* A **33** 021402
[82] Koop J and Deutschmann O 2009 Detailed surface reaction mechanism for Pt-catalyzed abatement of automotive exhaust gases *Appl. Catal.* B **91** 47–58
[83] Yuan M H, Chang C Y, Shie J L, Chang C C, Chen J H and Tsai W T 2010 Destruction of naphthalene via ozone-catalytic oxidation process over Pt/Al_2O_3 catalyst *J. Hazard. Mater.* **175** 809–15
[84] Prinetto F, Ghiotti G, Nova I, Lietti L, Tronconi E and Forzatti P 2001 FT-IR and TPD investigation of the NO_x storage properties of BaO/Al_2O_3 and $Pt-BaO/Al_2O_3$ catalysts *J. Phys. Chem.* B **105** 12732–45

[85] Yang X, Richards C and Adamovich I V 2023 Ammonia generation in Ns pulse and Ns pulse/RF discharges over a catalytic surface *Plasma Sources Sci. Technol.* **32** 064003
[86] Doherty F and Goldsmith B R 2023 Modeling plasma-induced surface charge effects on CO_2 activation by single atom catalysts supported on reducible and irreducible metal oxides *Plasma Sources Sci. Technol.* **32** 034004
[87] Neyts E C 2016 Plasma-surface interactions in plasma catalysis *Plasma Chem. Plasma Process.* **36** 185–212
[88] Bal K M, Huygh S, Bogaerts A and Neyts E C 2018 Effect of plasma-induced surface charging on catalytic processes: application to CO_2 activation *Plasma Sources Sci. Technol.* **27** 024001